Barium isotope (re-)equilibration in the barite-fluid system and its implications for marine barite archives

van Zuilen, Kirsten; Harrison, Anna L.; Stammeier, Jessica A.; Nagler, Thomas F.; Mavromatis, Vasileios

published in
Earth and Planetary Science Letters
2023

DOI (link to publisher)
10.1016/j.epsl.2023.118280

document version
Publisher's PDF, also known as Version of record

Earth and Planetary Science Letters 618 (2023) 118280

Contents lists available at ScienceDirect

Earth and Planetary Science Letters

journal homepage: www.elsevier.com/locate/epsl

Barium isotope (re-)equilibration in the barite-fluid system and its implications for marine barite archives

Kirsten van Zuilen [a,*,1], Anna L. Harrison [b,c], Jessica A. Stammeier [d], Thomas F. Nagler [c], Vasileios Mavromatis (Βασίλειος Μαυρομάτης) [b,c]

[a] Vrije Universiteit, De Boelelaan 1085, 1081 HV Amsterdam, the Netherlands
[b] Geosciences Environnement Toulouse (GET), Observatoire Midi-Pyrénées, Université de Toulouse, CNRS, IRD, UPS, 14 Avenue Edouard Belin, 31400 Toulouse, France
[c] Institute of Geological Sciences, University of Bern, Baltzerstr. 1+3, 3012 Bern, Switzerland
[d] Deutsches GeoForschungsZentrum GFZ, Telegrafenberg, 14473 Potsdam, Germany

ARTICLE INFO

Article history:
Received 17 April 2023
Received in revised form 9 June 2023
Accepted 13 June 2023
Available online 28 June 2023
Editor: A. Jacobson

Keywords:
barite
Ba isotopes
equilibrium fractionation
re-equilibration rates

ABSTRACT

Variations in the Ba isotopic composition of seawater are largely driven by the extent of barite precipitation in the marine photic zone and replenishment of Ba by upwelling and/or continental inputs. Pelagic barites offer a robust tool for tracing sources and sinks of Ba in the (paleo)ocean as they record these isotopic variations. Knowledge of the Ba isotope fractionation between barite and ambient waters is therefore imperative. Here, the Ba isotope fractionation between barite and Ba^{2+} (aq) under equilibrium conditions has been estimated by the three-isotope method with a ^{135}Ba-enriched reactive fluid. The estimated Ba isotope fractionation was $\Delta^{137/134}Ba_{Barite\text{-}Ba2+} = -0.07 \pm 0.08‰$. Textural observations of barite crystals recovered up to 756 days of reaction reveal smoothing of solid surfaces but also typical dissolution features such as development of pits and cracks. Thus, dissolution/re-precipitation is likely the mechanism controlling the observed isotope exchange that is facilitated by the further development of porosity in the crystals. Additionally, the isotope exchange in the experimental runs fits a second-order law yielding a surface normalized isotope exchange rate of $\sim 2.8 \times 10^{-10}$ mol/m^2/s. This exchange rate could theoretically result in complete isotope exchange between pelagic barite with a typical edge size of 1 µm and ambient seawater or pore fluid within years, altering the barite's Ba isotopic composition during settling towards the seafloor and/or after deposition in marine sediments. Although there is considerable uncertainty in extrapolating experimental results to natural conditions and longer time scales, the rapid rates of exchange observed experimentally over short timescales suggest that isotope exchange in pelagic barite should be considered during interpretation of the Ba isotope composition as a paleoarchive.

1. Introduction

Barium sulphate or barite ($BaSO_4$) is a naturally occurring mineral in marine environments that forms in the water column (pelagic barite), in hydrothermal or cold seep settings and as diagenetic barite from porewaters in marine sediments. Despite relatively high Ba^{2+} and SO_4^{2-} concentrations in seawater, modern oceans are undersaturated with respect to barite (Monnin and Cividini, 2006), prohibiting spontaneous precipitation of pelagic barite in the water column. Instead, it is assumed that precipitation occurs when organic matter is re-mineralised in the mesopelagic zone, typically between 200 and 600 m water depth (Horner et al., 2015; Bates et al., 2017). Upon remineralisation, Ba^{2+} associated to phytoplankton is released, allowing the nucleation of barite in microenvironments (Chow and Goldberg, 1960; Martinez-Ruiz et al., 2020). Thus, the formation of pelagic barite is indirectly linked to primary productivity (Dehairs et al., 1980; Paytan and Griffith, 2007). Furthermore, sedimentation of this mineral constitutes the major output of Ba from the oceans (Paytan and Kastner, 1996; Carter et al., 2020).

* Corresponding author.
E-mail address: kirsten.vanzuilen@shell.com (K. van Zuilen).
[1] Present address: Shell Global Solutions International B.V., Carel van Bylandtlaan 23, 2596HP The Hague, The Netherlands.

https://doi.org/10.1016/j.epsl.2023.118280
0012-821X/

Barite is characterized by very low solubility (Blount, 1977) and is considered stable under oxic conditions over geological timescales (Paytan and Griffith, 2007), making it a more robust archive compared to, for instance, carbonates. Over the last decade, it has been shown that changes in pelagic barite precipitation, hence primary productivity, and ocean circulation may manifest in variations in the Ba isotopic composition of seawater (e.g., Horner and Crockford, 2021). Barite precipitation is one of the main drivers, as barite preferentially takes up the lighter Ba isotopes (von Allmen et al., 2010), leaving seawater enriched in the heavier isotopes (e.g., Horner et al., 2015; Bates et al., 2017). Repletion of dissolved Ba in deep waters, on the other hand, lowers the $\delta^{137/134}$Ba values of seawater. The Ba isotopic composition of precipitating pelagic barite depends mainly on the isotopic composition of the ambient seawater. Barites have therefore the potential to capture and archive changes in marine Ba sources and cycling in the past (Bridgestock et al., 2018, 2019; Horner and Crockford, 2021).

Once deposited on the seafloor, barite preservation within marine sediments depends on the SO_4^{2-} concentration in pore waters. In oxygen-depleted sediment layers, biological activity results in reduction of sulphate that is used as an energy source and barite is dissolved (McManus et al., 1998, Paytan and Griffith, 2007). Dissolved Ba^{2+} subsequently diffuses within the sediment, and secondary, i.e., diagenetic, barite may form in oxic sediment layers where SO_4^{2-} is available (Torres et al., 1996). Although it can be assumed that dissolution of pelagic barite in the sediments is not accompanied by Ba isotope fractionation (van Zuilen et al., 2016b), fractionation is likely to happen during precipitation of diagenetic barite (von Allmen et al., 2010; Böttcher et al., 2018) and may also occur during diffusion of Ba^{2+} in the porewaters towards SO_4^{2-} rich layers (van Zuilen et al., 2016a). Consequently, it is likely that pore waters in marine sediments exhibit a large range in Ba isotope ratios (Pretet, 2013).

Apart from kinetic processes, isotope fractionation can occur upon isotope exchange in a mineral-fluid system under chemical equilibrium conditions, as was observed for Ba in carbonates (Mavromatis et al., 2016, 2020). Similar isotope exchange was further seen between carbonate minerals and fluid for metal isotopes such as Ca, Mg and Sr (e.g., Pearce et al., 2012; Mavromatis et al., 2017; Perez-Fernandez et al., 2017; Oelkers et al., 2018), but also for C and O (e.g., Dietzel et al., 2020; Harrison et al., 2021, 2022), as well as between silicate minerals and fluid (e.g., Liu et al., 2016; Stamm et al., 2019). The mechanisms behind isotope exchange in some cases can be clearly assigned to dissolution and reprecipitation reactions, particularly when a change in mineralogy (e.g., Harrison et al., 2021) or crystal morphology (e.g., Harrison et al., 2023) can be observed. However, isotope exchange can also occur without obvious changes of the mineral phase, composition or morphology (Gorski and Fantle, 2017). In the case of barite, previous studies have shown that isotope exchange traced with ^{133}Ba or ^{226}Ra is a rather rapid process that is not accompanied by changes in crystal morphology (e.g., Curti et al., 2010).

These previous observations of rapid isotope exchange between barite and aqueous Ba^{2+} call for an assessment of the stability of the primary Ba isotope signals in (pelagic) barite to support their reliable use as archives of past environmental conditions. In this study, we focus on Ba isotope exchange between natural barite from the Harz mountains (central Germany) and isotopically labelled aqueous Ba^{2+} under chemical equilibrium conditions. Isotope exchange rates and equilibrium isotope fractionation between mineral and aqueous fluids were experimentally investigated over ~25-month-long experiments. The results allow calculation of Ba isotope re-equilibration rates and generate insight on the fidelity of natural Ba isotope signatures of marine barites.

2. Materials and methods

The mechanisms of isotope exchange between barite and reactive fluid were evaluated using the three-isotope technique. Details of the experimental setup are given in the Supplement. In brief, ~0.050 g of powdered terrestrial gangue barite, with a grain size of about 30 to 60 µm and a reactive surface of 0.26 m^2/g (Fig. 1A), were placed in 17 individual reactors of 10 mL polypropylene vials. A solution was prepared from barium chloride dihydrate ($BaCl_2 \bullet 2H_2O$) and sodium chloride (NaCl) powders and deionised water and subsequently enriched in ^{135}Ba by addition of a known mass of a ^{135}Ba spike solution, resulting in an initial fluid with a $\delta^{135/134}$Ba value of 236.5‰ and a $\delta^{137/134}$Ba value of −0.02‰ (Table S2). To each reactor, ~10 g of the ^{135}Ba enriched solution were added and left to equilibrate with the barite for up to 756 days at room temperature. Each reactor contained ~2.2×10^{-4} mol Ba as solid phase compared to only 1.5×10^{-6} mol Ba in the aqueous solution. No sulphate was initially present in solution, causing minor dissolution of barite towards chemical equilibrium. The reactors were vigorously shaken approximately every second day. At selected time intervals over the experimental duration (see Table S1), individual reactors were sampled in their entirety.

Details of the analytical methods are given in the Supplement. Ba isotope data are presented in the delta notation:

$$\delta^{x/134}Ba\,[‰] = \left(\frac{{}^{x}Ba/{}^{134}Ba_{sample}}{{}^{x}Ba/{}^{134}Ba_{SRM\ 3104a}} - 1 \right) * 1000, \quad (1)$$

where x denotes 135 and 137, respectively. For the conversion of $\delta^{138/134}$Ba values from literature data that are used below to $\delta^{137/134}$Ba, a factor of 3/4 was applied.

3. Results

3.1. Chemical and isotopic composition of reactive fluids and solids

In the early stages of the mineral-fluid exchange experiments, the concentration of Ba in the reactive fluid decreased significantly from ~0.15 mM in the initially introduced stock solution to ~0.11 mM after 1724 hours (i.e., ~72 days) of reaction time and remained afterwards stable at 0.11 ± 0.01 mM until the end of the experiment (Fig. 2A; Table S1). Possible adsorption of dissolved Ba^{2+} onto the inner wall of the reaction vials, and potentially associated Ba isotope fractionation, was negligible within analytical uncertainty (see Supplement). The concentration of SO_4^{2-} was constant over the whole experiment at 0.0023 ± 0.0004 mM (Table S1). The supersaturation degree of the fluid with respect to barite (i.e., Ω_{Barite}) remained constant as well at a value of ~1.0 ± 0.1 (Fig. 2B; Table S1), denoting that during the whole duration of the experiment the solution was at chemical equilibrium with respect to barite.

Similar to the Ba concentration, the $\delta^{135/134}$Ba composition of the reactive fluid exhibited significant variations in the early stages of the experiments (Fig. 2C). Initially, $\delta^{135/134}Ba_{fluid}$ decreased rapidly from 236.5‰ in the stock solution to ~89‰ in sample BaSp1 after ~4 days of reaction time. Subsequently, $\delta^{135/134}Ba_{fluid}$ decreased further to a value of ~9‰ (sample BaSp8) up to day 86 (i.e., 2060 hours) of the experiment. After this time point and until the end of the experiment after 756 days, $\delta^{135/134}Ba_{fluid}$ decreased at a slower rate, achieving a final value of ~3‰. In contrast, considerably less variations were observed for $\delta^{137/134}Ba_{fluid}$, which varied around a value of 0.01 ± 0.09‰ in all the fluid samples (Table S2).

Mirroring the fluid, the $\delta^{135/134}$Ba values of the barite became more positive with time (Fig. 2D). The barite seed used in this

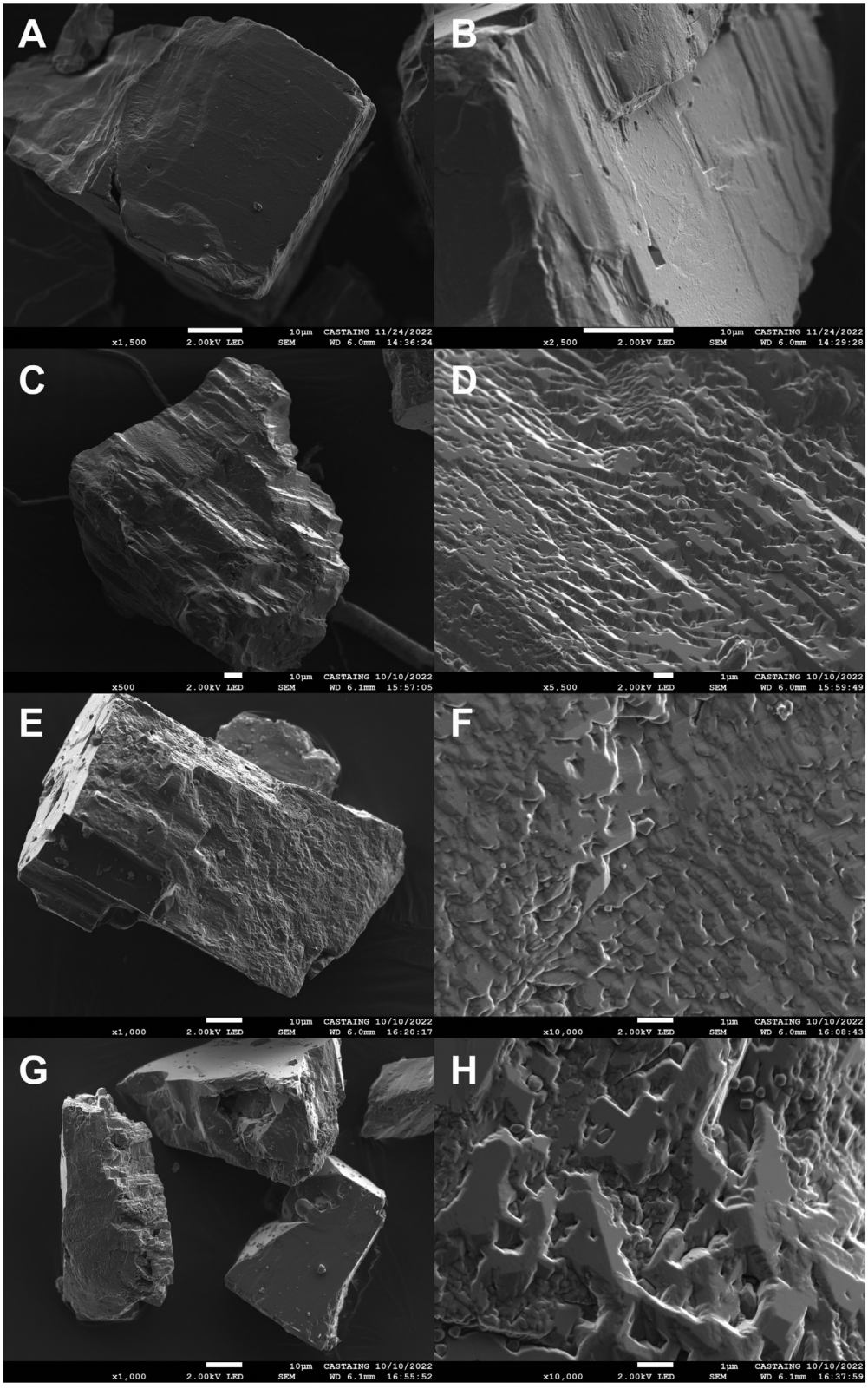

Fig. 1. Scanning electron microphotographs of characteristic barite seed grains (A and B), and barite grains recovered after ~135 days (C and D), ~326 days (E and F) and 756 days (G and H).

study has a $\delta^{135/134}$Ba value of -0.04 ± 0.09‰ ($2s_p$, Table S2) which rapidly increased to 0.08 ± 0.09‰ in sample BaSp1 (~4 days) and obtained a value of 0.17 ± 0.09‰ at the end of the experiments after 756 days. The significant increase in $\delta^{135/134}Ba_{solid}$ can be assigned to isotopic exchange with the artificially ^{135}Ba-enriched reactive fluid, as discussed later. The $\delta^{137/134}Ba_{solid}$ value, on the other hand, remained constant within analytical uncertainty over the experiment (Table S2).

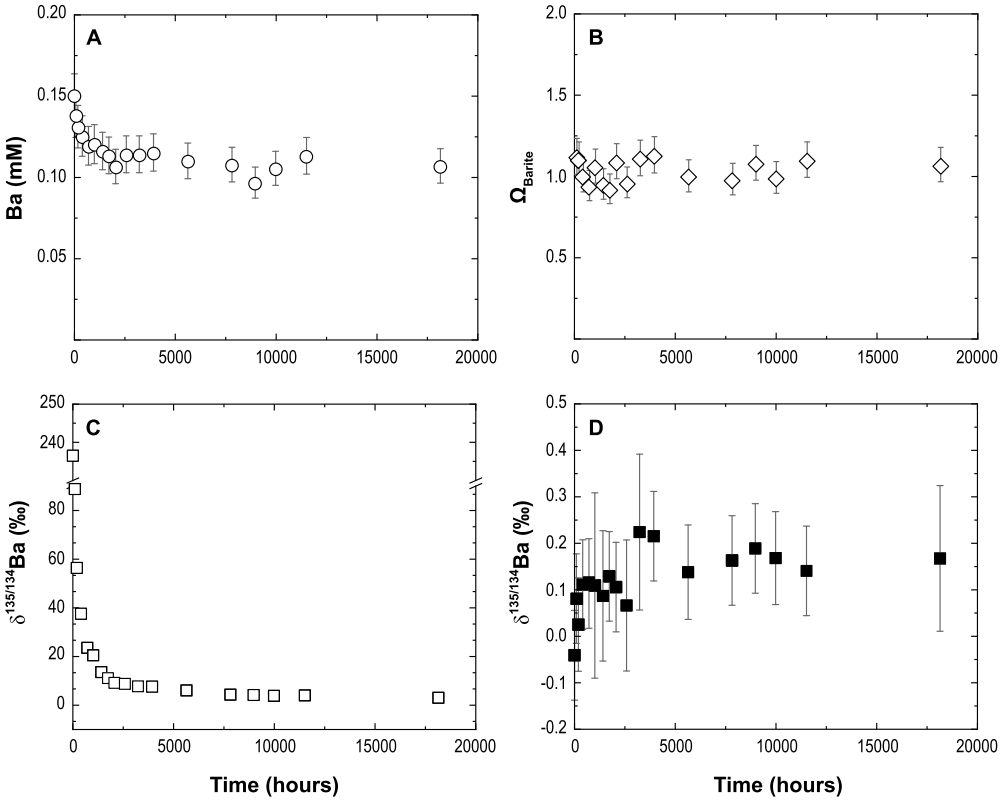

Fig. 2. Temporal evolution of A) aqueous Ba concentration, B) degree of supersaturation of the fluid with respect to barite, C) $\delta^{135/134}$Ba composition of the aqueous phase and D) $\delta^{135/134}$Ba composition of the reacted barite. If not shown, error bars are smaller than symbol size.

3.2. Textural characterization of solids

Scanning Electron Microscopy (SEM) images of the barite used in the experiments and selected samples of the recovered material can be seen in Fig. 1. The size of the grains recovered from the reactors appears to be similar to that of the seed as depicted in Fig. 1A. Interestingly, however, SEM images reveal development of surface features typical for dissolution processes (e.g., development of pits and cracks; Figs. 1D, 1F and 1H), but also other regions of the same grain appear smooth and flat compared to the rough surfaces of the barite seeds (Fig. 1B). Overall, the SEM images presented in Fig. 1 suggest continuous development of the surface characteristics of the barite used in this study during the entire duration of the experiments.

3.3. Calculation of Ba isotope exchange and isotope fractionation between solid and Ba^{2+}(aq)

The degree of isotope exchange (F) has been calculated similar to earlier works (e.g., Cole and Chakraborty, 2001; Johnson et al., 2002; Stamm et al., 2019), using the expression:

$$F = \frac{(\delta_t - \delta_i)}{(\delta_e - \delta_i)} \quad (2)$$

where δ_t denotes the isotopic composition (in this case $\delta^{135/34}$Ba) of either one of the phases at any time, t, during the isotope exchange reaction, and δ_i and δ_e describe the initial and equilibrium isotope composition of this phase, respectively. The parameter F ranges from 0 to 1 as isotopic equilibrium is attained. Note here that F quantifies the deviation from a complete isotope exchange between the two phases, but Eq. (2) does not quantify the number of atoms that have been mixed, which depends on the relative amounts of the element in the fluid versus the solid phase (Handler et al., 2014; Frierdich et al., 2015). According to Zheng et al. (2016), the parameter F can be used to estimate kinetics of isotope exchange (e.g., Cole and Chakraborty, 2001) and to evaluate kinetic isotope effects during isotope exchange (e.g., Frierdich et al., 2014a, 2014b).

In a two-component system, δ_e can be derived from the mass balance constraints (Zheng et al., 2016) and calculated from:

$$\delta_e = \delta_{mean} - \left(\frac{N_{solid}}{N_{solid} + N_{fluid}}\right) \times \Delta_{eq,solid-fluid} \quad (3)$$

where δ_{mean} in this study stands for the averaged Ba isotope composition of the system, $\Delta_{eq,solid-fluid}$ designates the equilibrium isotope fractionation factor between the $BaSO_4$ solids and the aqueous phase, and N_{solid} and N_{fluid} denote the moles of Ba in the solid and aqueous phase, respectively. According to Zheng et al. (2016), if the $\Delta_{eq,solid-fluid}$ is unknown, it can be estimated from an iterative fit of the experimental data. As can be seen in Table S1, parameter F reaches values between 0.63 in sample BaSp1 and 0.99 at the end of the runs (sample BaSp17) when calculated from the changes in the isotopic composition of the fluid. Note here that use of the aqueous data in this study has been chosen because the $\delta^{135/34}Ba_{fluid}$ value exhibits a significant temporal variation (Fig. 2C) that is not observed for $\delta^{135/34}Ba_{solid}$ (Fig. 2D), but also because the fluid can be considered as a homogeneous phase, which is not the case for the solid.

Owing to the absence of Ba complexation in the aqueous phase, Ba isotope fractionation between barite and Ba^{2+} (aq) can be estimated with the aid of Fig. 3. In this figure, the non-spiked $\delta^{137/134}$Ba isotope compositions of the fluid and solid phase have been plotted as a function of the degree of isotope exchange F calculated based on changes in the aqueous $\delta^{135/134}$Ba composition. Under isotope equilibrium conditions, i.e., $F = 1$, Ba isotope fractionation has been estimated as:

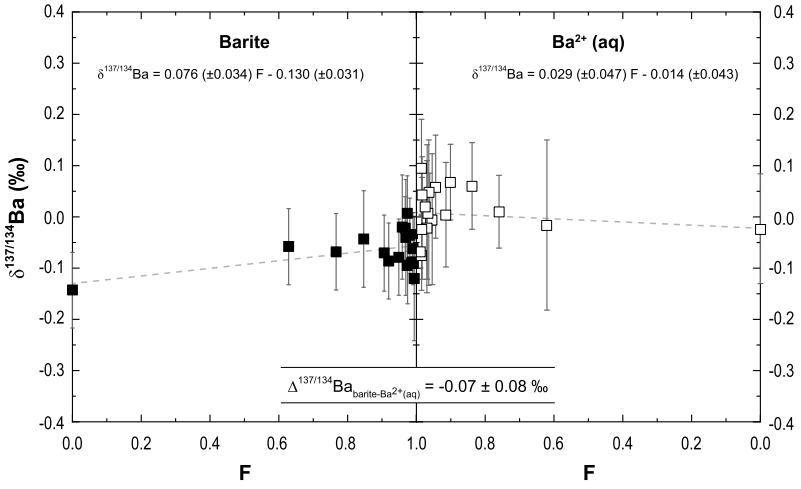

Fig. 3. Barium isotope composition of barite (black squares) and fluids (white squares) as a function of the degree of isotope exchange, F, during the course of the experimental runs. Linear extrapolations to $F = 1$ have been used to estimate equilibrium Ba isotope fractionation at 25 °C.

$$\Delta^{137/134}\mathrm{Ba}_{\mathrm{Barite\text{-}Ba2+(aq)}} = \delta^{137/134}\mathrm{Ba}_{\mathrm{Barite}} - \delta^{137/134}\mathrm{Ba}_{\mathrm{Ba2+(aq)}} \quad (4)$$

The estimated equilibrium $\Delta^{137/134}\mathrm{Ba}_{\mathrm{Barite\text{-}Ba2+(aq)}}$ value is -0.07 ± 0.08‰.

3.4. Kinetics of Ba isotope exchange

The use of a ^{135}Ba spike in the experimental runs allows for estimation of the kinetics of isotope exchange. In a similar manner to that of O and Fe exchange (Cole and Chakraborty, 2001; Johnson et al., 2002), the rate of isotope exchange can be quantified using

$$\frac{-d(1-F)}{dt} = k_n(1-F)^n \quad (5)$$

where k_n represents the rate constant of reaction order n. For barite dissolution and precipitation, earlier works have shown that the reaction can be of first or second order (e.g., Christy and Putnis, 1993; Zhen-Wu et al., 2016; Kang et al., 2022).

The integrated form of this rate equation can be written as

$$\ln(1-F) = -k_1 t \quad (6)$$

for $n = 1$
or as

$$\frac{F}{(1-F)} = k_2 t \quad (7)$$

for $n = 2$.

By fitting the experimental values of F to Eqs. (6) and (7), the isotope exchange rate constants for first and second order reactions can be quantified, respectively.

4. Discussion

4.1. Kinetics of Ba isotope exchange and reactivity of barite

An interesting observation in the experimental runs is the rapid change of the $\delta^{135/134}\mathrm{Ba}_{\mathrm{fluid}}$ value, which after 90 hours of reaction already obtained a value of ~89‰, compared to the initial composition of the fluid of 236.5‰. The extent of Ba exchange can be approximated by mass balance by treating the isotopic exchange as a mixture of two endmembers:

$$\delta^{135/134}Ba_t = \delta^{135/134}Ba_i * (1 - f_{barite}) + \delta^{135/134}Ba_{barite} * f_{barite} \quad (8)$$

where $\delta^{135/134}Ba_t$ and $\delta^{135/134}Ba_i$ are the Ba isotope composition of the reactive fluid at time t, and that of the initial solution, respectively, $\delta^{135/134}Ba_{barite}$ is the isotopic composition of the initial barite and f_{barite} the fraction of Ba in the reactive fluid derived from barite. Solving Eq. (8) for f_{barite} within the first 90 hours of the experimental runs reveals that about 62% of Ba in the reactive fluid is derived from barite in order to reduce the $\delta^{135/134}\mathrm{Ba}_{\mathrm{fluid}}$ value to ~89‰, assuming the Ba released from the solid maintained its initial composition. In other words, this calculation suggests that $\sim 9.3 \times 10^{-7}$ mol Ba of a 0.15 mM Ba solution with a volume of 10 mL was derived from barite. Considering that 0.05 g of barite in each reactor had a total surface of 0.013 m^2 and that the barite unit cells occur as ideal cubes with an edge of 7.03 Å, about 2.63×10^{16} unit cells were exposed to the fluid, containing $\sim 1.05 \times 10^{17}$ atoms or 1.75×10^{-7} moles of Ba. Although this number of moles in the surface layer is about six times lower compared to the amount of exchanged Ba as estimated by Eq. (8), it does not necessarily imply that more than the surface barite layer was exchanged with the fluid within the first 90 hours of the experimental run. Additional Ba from the solid was most likely also contributed from the dissolution of grain surfaces. Indeed, barite seeds that were originally in the reactor partially dissolved for chemical equilibrium to be achieved, as the initial solution used in the experimental runs did not contain SO_4^{2-}. In order for the solution to achieve a SO_4^{2-} concentration of ~0.002 mM (Table S1), about 2×10^{-8} mols of Ba^{2+} and SO_4^{2-} were derived from the solid, considering that each reactor contained 10 mL of reactive fluid. This amount of Ba, however, is ~47 times lower compared to the amount estimated to have been sourced from the solid with Eq. (8). It is therefore unlikely that net barite dissolution significantly contributed to the change in Ba isotope composition of the fluid in the experimental runs. Note here that, recently, Middleton et al. (2023a) argued that there is fractionation during dissolution of barite using as an example earlier works on iron oxides (e.g., Wiederhold et al., 2006; Skulan et al., 2002). In these works, however, the mineral-fluid system is far from chemical equilibrium (i.e., $\Omega_{\mathrm{mineral}} \ll 1$) and breaking of the isotopically lighter Me-O bonds in the solid phase is energetically favoured, producing in all cases enrichment of the fluid with the lighter isotopes. This process has been also recognized at the initial stages of silicate (Oelkers et al., 2015; Maher et al., 2016) and carbonate (Oelkers et al., 2018) mineral dissolution, but is unlikely to operate at near chemical equilibrium conditions where the rate of dissolution is equal to that of precipitation, as it is dictated by the dynamic mineral-fluid

equilibrium chemical/isotope exchange (Schott et al., 2009; Oelkers et al., 2019).

During the first 1724 hours of the experiment, the aqueous Ba concentration of the fluids decreased from ~0.15 mM in the synthetic stock solution to a steady state concentration of 0.11 ± 0.01 mM. This decrease in aqueous Ba is not accompanied by a stoichiometric decrease in SO_4^{2-} (aq), as would be expected for the precipitation reaction of barite, and, based on adsorption experiments (Fig. S1), Ba loss due to sorption of Ba to the reactor walls is unlikely. Instead, it might rather be attributed to a replacement reaction with another ion, likely Na, present in barite as a chemical impurity in the form of Na_2SO_4. This hypothesis is supported by the formation model of barite in the Harz mountains, from where the barite used in this study originated. In this locality, barite was deposited from highly saline, NaCl-$CaCl_2$-rich brines during the Mesozoic (De Graaf et al., 2020 and references therein). If the exchange with Na was solely responsible for the decrease in aqueous Ba concentration, about 6×10^{-7} mol of Na would have been released into the fluid over the first 407 hours (i.e., ~17 days). This constitutes less than 1% of the total amount of Na in the fluid (Table S1) and is undetectable within the analytical uncertainties of the Na concentration analysis.

Hence, despite the initial variation in Ba concentration, it can be considered that the barite-fluid system effectively attained bulk chemical equilibrium within ~90 h (sample BaSp1) of the experiment, based on attainment of stable SO_4^{2-} concentrations and the calculated $\Omega_{Barite} = \sim 1$ (Fig. 2B). In addition, the moles of Ba removed from solution within the first 90 h (i.e., $\sim 1.2 \times 10^{-7}$ mol) represent ~8% of the mass of initial Ba in the fluid, which does not account for the ~62% exchange between fluid and solid required to shift the fluid isotopic composition from 236.5‰ to 88.85‰. However, it should be noted that Eq. (8) does not account for continuous exchange between fluid and solid (i.e., only end member exchange) and is thus subject to uncertainty.

The isotope exchange between barite and fluid in the experiments of this study was approximated with parameter F derived from Eq. (2), which represents the approach towards isotopic equilibrium rather than the total mass exchanged, and was higher than 90% after ~30 days (i.e., 715 hours) of reaction and reached 99% at the end of the runs (Table S1). This high degree of isotope exchange suggests the mineral-fluid system obtained near isotopic equilibrium conditions. Interestingly, however, F and $\delta^{135/134}Ba_{fluid}$ continuously evolve during the runs, denoting continuous exchange of Ba between barite and fluid under chemical equilibrium conditions. Notably, although the $\delta^{135/134}Ba_{fluid}$ of the final sample after 756 days (BaSp17; 3.06‰) is significantly lower compared to the initial stock solution (i.e., 236.5‰), it has not achieved complete isotope exchange, which would yield a value of 1.55‰ based on mass balance.

The rate of isotope exchange was further quantified using F and exhibits a best-fit to a second-order rate law that is described by Eq. (7) (Fig. 4). A second-order rate law is consistent with barite precipitation (Christy and Putnis, 1993), suggesting that under chemical equilibrium the backward reaction (i.e., precipitation) controls the isotopic composition of the fluid. The surface-normalized rate of the second-order fit is 2.8×10^{-10} mol/m^2/s, estimated by the linear fit of the data using Eq. (7), which was corrected for the Ba concentration in the reactors and the barite surface area. The estimated exchange rate is in good agreement with the measured barite precipitation rate of $10^{-9.2}$ mol/m^2/s and about 1.5 orders of magnitude slower than the dissolution rate (i.e., $10^{-8.05}$ mol/m^2/s) reported by Zhen-Wu et al. (2016) for experiments conducted in de-ionized water. The relatively good agreement between isotope exchange rate and precipitation rate is consistent with a dissolution-precipitation mechanism controlling Ba isotope exchange. Moreover, the estimated isotope exchange

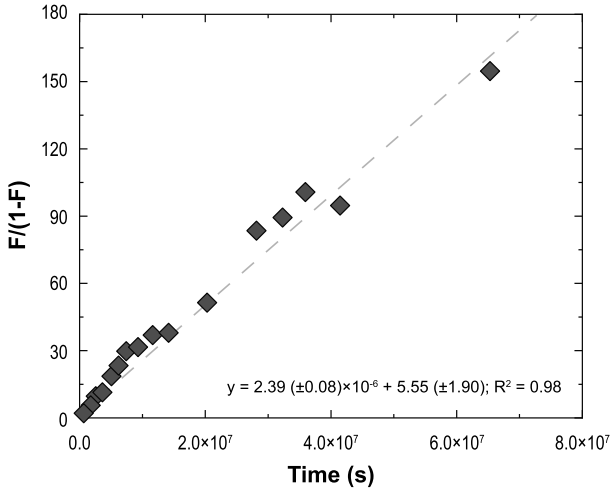

Fig. 4. Second order fit of isotope exchange data estimated with the aid of Eq. (7). The rate constant derived from this figure, expressed in s^{-1}, is dependent on the solid-fluid ratio. It can be normalized to the solid BET surface area per kg H_2O using: k (in mol/m^2/s) = k (in 1/s) × C_{Ba}/S, where C_{Ba} stands for equilibrium Ba concentration in mol/kg H_2O and S is the BET solid surface area (m^2) per kg H_2O.

rate is in excellent agreement with that reported by Curti et al. (2010) for barite recrystallization experiments conducted in the presence of ^{133}Ba in de-ionized water. In their experiments, which lasted ~400 days, Curti et al. (2010) reported barite recrystallization rates of $5.67 \pm 2.55 \times 10^{-10}$ mol/m^2/s. Curti et al. (2010), however, reported up to one order of magnitude lower recrystallization rates in the presence of background electrolytes (e.g., NaCl, Na_2SO_4 and/or $NaHCO_3$). The observed surface normalized recrystallization rate in the present study is similar to the attachment/detachment rates of Ba isotopes on barite surface that was recently reported by Kang et al. (2022) in experiments conducted under chemical equilibrium conditions. According to Kang et al. (2022), the rate of Ba attachment on barite surface is equal to that of detachment and depends on the Ba^{2+}/SO_4^{2-} ratio of the reactive solution, with higher ratios yielding faster attachment rates. A direct comparison with the runs of the present study, in which $Ba^{2+}/SO_4^{2-} > 50$, suggests that the estimated recrystallization rate is ~0.5 orders of magnitude lower compared to the attachment rate reported in Kang et al. (2022) for similar Ba^{2+}/SO_4^{2-} ratios.

The exchange of Ba isotopes between barite and fluid was not limited to the first 90 hours (i.e., ~4 days) of the experiment. A rapid decrease in the $\delta^{135/134}Ba_{fluid}$ value was measured up to ~100 days (BaSp9) followed by a lower but measurable rate of decrease until the end of the experiments at 756 days (Fig. 2). Applying Eq. (8) to the final timepoint of the experiment at 756 days indicates that 1.49×10^{-6} moles, corresponding to 98.7% of the Ba in the fluid and 0.7% of Ba in the solid, were exchanged (Fig. 5). This mass balance approach to estimate the extent of exchange (Eq. (8)), however, neglects the changing $\delta^{135/134}Ba_{fluid}$ composition over time. To account for the changing fluid composition, a time dependent mass balance was estimated, and thus Eq. (8) was modified as:

$$\delta^{135/134}Ba_t = \delta^{135/134}Ba_{t-1} * (1 - f_{barite}) + \delta^{135/134}Ba_{barite} * f_{barite} \quad (9)$$

where $\delta^{135/134}Ba_{t-1}$ is the isotopic composition of the fluid at the sampling point immediately before t. The application of Eq. (9) to the measured data rather than Eq. (8) suggests a greater extent of exchange, with up to 2.5% of Ba in the solid affected by exchange with the fluid (Fig. 5). However, this model still assumes

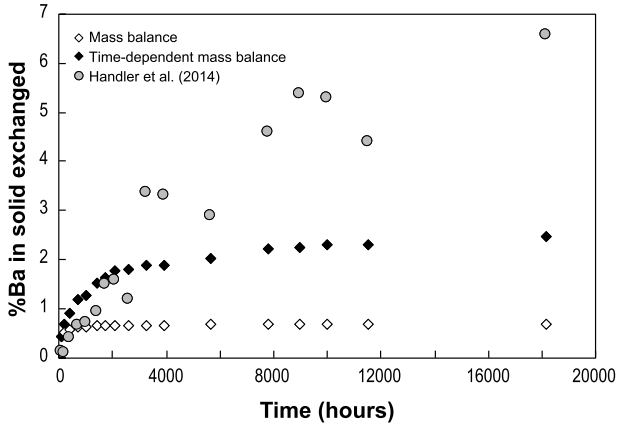

Fig. 5. Extent of Ba in the solid exchanged with the fluid versus time using different models. "Mass balance" is the results of Eq. (8); "Time-dependent mass balance" is the results of Eq. (9); "Handler et al. (2014)" is the results of Eq. (10) based on Handler et al. (2014).

that the solid does not continue to exchange with the fluid after initial exchange, but only that the composition of the fluid is changing. Alternatively, a previous study by Handler et al. (2014) applied a similar approach to account for a dynamic fluid and solid composition and the Fe isotope fractionation between goethite and fluid during Fe exchange, modified here for Ba isotope exchange between barite and aqueous Ba (Eqs. (10)-(12)):

$$\%Ba\ in\ barite\ exchange = \frac{\left[\left(\delta^{135/134}Ba_{barite,t} + w_{barite}\right) - \delta^{135/134}Ba_{barite,i}\right]}{\left[\left(\delta^{135/134}Ba_{t} - w_{Ba}\right) - \delta^{135/134}Ba_{barite,i}\right]} * 100 \quad (10)$$

$$w_{barite} = F \times \Delta^{137/134}\mathrm{Ba}_{\mathrm{barite-Ba^{2+}}} \times \left(1 - \frac{N_{barite}}{N_{Ba} + N_{barite}}\right) \quad (11)$$

$$w_{Ba} = F \times \Delta^{137/134}\mathrm{Ba}_{\mathrm{barite-Ba^{2+}}} \times \left(1 - \frac{N_{Ba}}{N_{Ba} + N_{barite}}\right) \quad (12)$$

where $\delta^{135/134}Ba_{barite,i}$ and $\delta^{135/134}Ba_{barite,t}$ are the initial and time t isotopic composition of Ba in barite, respectively, N_{barite} is the moles of Ba in barite, and N_{Ba} is the moles of Ba in the fluid. The approach by Handler et al. (2014) suggests a greater extent of Ba exchange than the simple mass balance model (Eq. (8)) with 6.6% exchange of the solid (Fig. 5) and more than complete cycling of the fluid reservoir (933.8% exchange). The greater extent of exchange implied by Eqs. (9) and (10) reflects the cumulative effect of exchange between solid and fluid at each time step, rather than a single mixing event of endmembers. Although the precise extent of exchange between fluid and solid is difficult to quantify and model-dependent (Fig. 5; Gorski and Fantle, 2017), it is clear that extensive exchange of isotopes, extending beyond the surface of barite, can occur on rapid timescales, and thus the potential for alteration of isotopic composition of barite is high. The significant fluid-solid exchange implied by the alteration of fluid isotope composition is consistent with the extensive alteration of the barite surface as depicted in Fig. 1. Although the SEM images do not provide evidence for significant change in grain size between seed material and reacted barite in sample BaSp17 (756 days), development of features typical of dissolution processes (i.e., pits, pores and cracks) were observed (Fig. 1H), in addition to features typical of mineral growth, such as smoothing of surfaces and filling of cracks. These features denote the transfer of matter from the surfaces with excess surface free energy (affected by defects, heterogeneities, etc.) to zones of lower surface free energy and are likely attributable to a defect-driven Ostwald ripening process (Zhang et al., 2022). Ostwald ripening has been proposed as a mechanism for the exchange of isotopes between solutions and solids in previous isotope exchange studies (Harrison et al., 2022; Géhin et al., 2021). As can be seen in Fig. 1H, dissolution and precipitation features can occur on the same grain, suggesting that dissolution and re-precipitation drives the isotope exchange observed in the barite-fluid system, likely additionally promoted by the development of microporosity that facilitates extensive mass exchange between fluid and solid, and the slight disequilibrium induced by chemical impurities in the barite.

4.2. Equilibrium Ba isotope fractionation between barite and fluid

As can be seen in Fig. 3, under isotopic equilibrium conditions, the lighter Ba isotopes are preferentially incorporated in barite, with an estimated $\Delta^{137/134}\mathrm{Ba}_{\mathrm{Barite\text{-}Ba2+(aq)}}$ value of $-0.07 \pm 0.08‰$. This fractionation is in excellent agreement with the $\Delta^{137/134}\mathrm{Ba}_{\mathrm{Barite\text{-}Ba2+(aq)}}$ value of $-0.08 \pm 0.04‰$ determined by Middleton et al. (2023a). The observed enrichment of the lighter isotopes in barite is consistent with the general rule that ions with larger isotopic masses will tend to accumulate in the phase with the shorter and/or stronger bond (Schauble, 2004). In the aqueous phase, Ba is coordinated to about eight H_2O molecules with an average Ba-O bond length of 2.79 Å (Persson et al., 1995). In contrast, Ba in barite is coordinated to twelve oxygen molecules with an average Ba-O bond length of ~2.85 Å (Finch et al., 2010). It is likely that both the change in coordination and the variation in the bonding environment contribute to the enrichment of the solid phase in the lighter ^{134}Ba isotope. For example, the anhydrous barium carbonate mineral witherite (i.e., $BaCO_3$) is also enriched in the lighter Ba isotopes under near isotopic equilibrium conditions (Mavromatis et al., 2016). In witherite, Ba is coordinated to nine oxygen molecules with an average Ba-O bond length of 2.80 Å. In contrast, the Ba bonding environment in aragonite displays a Ba-O bond length of ~2.75 Å, which is shorter compared to that of the aqueous phase. Thus, aragonite is enriched in the heavier isotopes at near equilibrium conditions (Mavromatis et al., 2020; Wang et al., 2021).

The theoretical estimation of Ba isotope fractionation between barite and Ba^{2+}(aq) presented recently by Wang et al. (2021) comes in good agreement with the experimental findings of this study. Using first principles calculations based on density functional theory (DFT), Wang et al. (2021) estimated an enrichment of the lighter Ba isotopes in the solid phase under equilibrium conditions with an estimated Ba isotope fractionation of $-0.17 \pm 0.03‰$ in $\delta^{137/134}$Ba at 27 °C. Moreover, similar Ba isotope fractionation factors have been reported by von Allmen et al. (2010) and Böttcher et al. (2018) in experiments where barite was nucleated from solution or formed slowly through dissolution of gypsum in a Ba-bearing solution. These two earlier studies reported $\Delta^{137/134}\mathrm{Ba}_{\mathrm{Barite\text{-}Ba2+(aq)}}$ values that are somewhat larger compared to the findings of this work, averaging at $-0.24 \pm 0.03‰$. Although it is unclear what controls the observed enrichment in the lighter Ba isotopes of barite in the study by Böttcher et al. (2018), where mineral nucleation occurred at low supersaturations of the fluid with respect to barite, it is likely that the difference to this work is associated with dehydration kinetics of the aqueous Ba^{2+} ion. Indeed, molecular dynamic simulations by Hofmann et al. (2012) suggest that dehydration of aqueous Ba^{2+} can produce isotopic variations as large as $-1.1 \pm 0.2‰$. Note that dehydration of the aqueous ion is prerequisite for the incorporation of a divalent cation in an anhydrous mineral phase (Mavromatis et al., 2013; Schott et al., 2016). Indeed, isotope fractionation related to kinetics of aqueous ion dehydration has been earlier used to explain non-equilibrium fractionation for alkaline earth metals such as Ca and Sr (e.g., Tang et al., 2008; Mavromatis et al., 2017).

4.3. Implications for the preservation of Ba isotopic compositions in marine barites

In agreement with previous studies, the here presented results suggest that, under chemical equilibrium, isotope exchange between barite and fluid occurs rapidly (e.g., Curti et al., 2010; Heberling et al., 2018; Kang et al., 2022). This rapid isotope exchange has also been observed for other minerals when in contact with a fluid, e.g., for C, O and Ca isotopes in carbonates of both abiotic and biogenic origin (e.g., Bernard et al., 2017; Oelkers et al., 2019; Cisneros-Lazaro et al., 2022; Harrison et al., 2022). The process of isotope exchange that occurs at chemical equilibrium could proceed via Ostwald ripening and results in either observable alteration of crystal surfaces and morphology, such as documented for Ca isotope exchange between aragonite and fluid (Harrison et al., 2023), or might occur without obvious changes to the crystal surface (e.g., Gorski and Fantle, 2017; Harrison et al., 2022). For example, in Ca isotope exchange experiments between nanocrystalline calcite and reactive fluid of Harrison et al. (2023), the grain size did not increase during 4 months of reaction despite measurable Ca isotope exchange. Similar observations were made for B isotope exchange between amorphous-derived nanocrystalline calcite and fluid for over two years (Mavromatis et al., 2021). In the case of barite, Curti et al. (2010) report that after 18 months of reaction, the solids exhibit reduction in roughness and an evolution of crystal morphology towards more regular forms without changes in average grain size and argued that Ostwald ripening cannot be a possible exchange mechanism in their runs. Nevertheless, Ostwald ripening may be possible without obvious changes to grain size if driven by defects at crystal surfaces (e.g., Zhang et al., 2022; Harrison et al., 2023; Géhin et al., 2021). The SEM images of this study (Fig. 1) similarly suggest no change in the grain size, however surface features on grains point towards active dissolution/re-precipitation mechanism controlling isotope exchange between barite and fluid. Importantly, altogether these observations suggest that the Ba isotope composition of barite is likely to be modified when in contact with a fluid of different composition within rapid time frames, irrespective of the mechanism.

The possibility of Ba isotope re-equilibration in barite is of great importance for the use of pelagic barite as an archive for marine Ba isotope variations. The $\Delta^{137/134}Ba_{Barite\text{-}Ba2+(aq)}$ at equilibrium estimated in this study (i.e., -0.07 ± 0.08‰) is somewhat smaller compared to that reported in von Allmen et al. (2010) and Böttcher et al. (2018) which average to $\Delta^{137/134}Ba_{Barite\text{-}Ba2+(aq)} = -0.24 \pm 0.03$‰. This average value determined experimentally is yet significantly smaller compared to what mass balance calculations of marine Ba cycle would predict for the barite-fluid system. Indeed, mass balance considerations of data from North and South Atlantic (Horner et al., 2015; Bates et al., 2017) and global seawater (Hsieh and Henderson, 2017), mass balanced values from core sediments (Bridgestock et al., 2018) and in-situ collected particles from Lake Superior (Horner et al., 2017) presented by Horner and Crockford (2021) suggest a $\Delta^{137/134}Ba_{Barite\text{-}Ba2+(aq)}$ of around -0.37‰. This difference between experimental data and natural samples, which actually increases if the $\Delta^{137/134}Ba_{Barite\text{-}Ba2+(aq)}$ value estimated in this study is considered, implies that a process that yields fractionation of Ba isotopes between barite and fluid is not taken into account. Horner and Crockford (2021) suggested that possible explanations include growth kinetics and complexation with organic/inorganic ligands. Yet, based on the rapid exchange of Ba isotopes observed in several studies, it is interesting to explore whether recrystallization can explain part of the variation between experiments and natural observations. For this exercise, the rate of isotope re-equilibration is examined assuming a barite crystal of 1 µm edge size that is typical for suspended particles (Dehairs et al., 1980) and the estimated, surface-normalised recrystallization rate obtained from Fig. 4 (i.e., $\sim 3\times10^{-10}$ mol/m^2/s). For this calculation it is assumed that barite has an initial $\delta^{137/134}Ba_{Barite}$ value of 0.45‰, which reflects formation from surface North Pacific waters without any fractionation, and is allowed to equilibrate with an infinite fluid reservoir with a $\delta^{137/134}Ba_{fluid}$ value of 0.16‰, representing deep ocean water below 1000 m depth (e.g., Horner and Crockford, 2021). The results of this calculation (Fig. 6A) suggest that, with the recrystallization rate measured in this study, complete isotope exchange to a $\delta^{137/134}Ba_{Barite}$ value of 0.16‰ requires only ~1.7 years. Of course, this exchange rate estimate does not necessarily reflect Ba isotope re-equilibration rates in an oceanic system due to potential impacts of fluid composition and temperature. Indeed, slower recrystallization rates up to an order of magnitude (i.e., $\sim 3 \times 10^{-11}$ mol/m^2/s) have been reported by Curti et al. (2010) in the presence of HCO_3^- in the background electrolyte and higher SO_4^{2-} concentration compared to this study. Similarly, Middleton et al. (2023a) observed recrystallisation rates between ~ 0.5 and 5.3×10^{-11} mol/m^2/s in artificial seawater, and even lower rates of $\sim 1 \times 10^{-12}$ mol/m^2/s were calculated for experiments using filtered seawater (Middleton et al., 2023b). In the latter case, Middleton et al. (2023b) assumed that dissolved organic matter may inhibit the reactivity of dissolved Ba. The re-equilibration calculation presented here

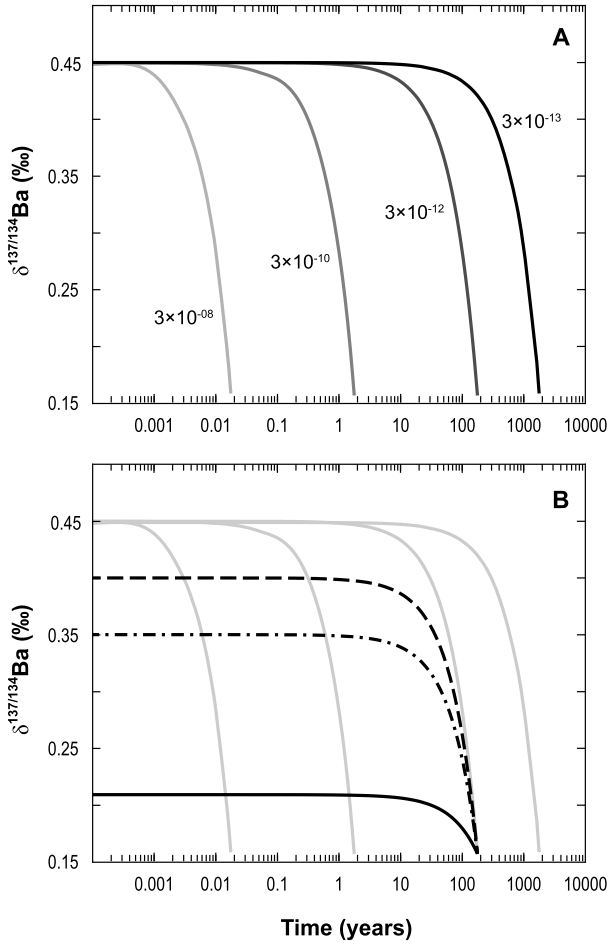

Fig. 6. Temporal evolution of Ba isotope composition of an ideal barite cube with 1 µm edge size using A) a range of re-equilibration rates between 3×10^{-8} and 3×10^{-13} mol/m^2/s. Time for complete re-equilibration ranges between 4 days and 1750 years. B) A re-equilibration rate of 3×10^{-12} mol/m^2/s was used and initial Ba isotope fractionation was assumed during precipitation of an ideal pelagic barite cube between surface seawater ($\delta^{137/134}Ba = 0.45$‰) with $\Delta^{137/134}Ba_{Barite\text{-}seawater}$ of -0.05, -0.10 (dashed lines) and -0.24‰ (solid black line; von Allmen et al., 2010, Böttcher et al., 2018). Curves from Fig. 6A are given as reference (grey).

furthermore assumes an ideal barite cube without development of porosity, which would increase surface area and subsequently shorten isotope re-equilibration. In order to consider these processes in Fig. 6A, results of Ba isotope re-equilibration estimated with rates in the range of 3×10^{-8} to 3×10^{-13} mol/m^2/s are presented, yielding exchange times ranging from 4.4 days to 1750 years, respectively. It should further be noted that the lower temperatures of ambient ocean water will presumably result in somewhat lower exchange rates compared to laboratory experiments at room temperature. Nevertheless, these estimations suggest that Ba isotope re-equilibration can occur rapidly, on timescales of days to hundreds of years, for micron-scale pelagic barite.

The results presented in Fig. 6A consider only isotope exchange and neglect isotope fractionation during pelagic barite nucleation. Assuming that precipitation of barite is accompanied by a fractionation of up to −0.24‰ (von Allmen et al., 2010; Böttcher et al., 2018), the solid ($\delta^{137/134}Ba_{Barite} = +0.21‰$) is allowed to equilibrate with an infinite fluid reservoir with $\delta^{137/134}Ba_{Seawater} = +0.16‰$ and a recrystallization rate of 3×10^{-12} mol/m^2/s (Fig. 6B). Note that the experiments by von Allmen et al. (2010) and Böttcher et al. (2018) were conducted under laboratory conditions (i.e., precipitation in strongly supersaturated solutions and in the presence of methanol, respectively) that are not representative for natural conditions and that reaction kinetics in the ocean might be slower. Therefore, isotope re-equilibration was also modelled for systems with $\Delta^{137/134}Ba_{Barite\text{-}seawater}$ of −0.05 and −0.10‰. In all cases, the barite crystal reached complete isotope exchange after 175 years (Fig. 6B). Assuming that re-equilibration is accompanied by equilibrium fractionation ($\Delta^{137/134}Ba_{Barite\text{-}Ba2+(aq)}$) of about −0.07‰, the resulting barite crystal might eventually have a $\delta^{137/134}Ba_{Barite}$ value <0.16‰.

How long barite particles remain in the ocean water column is dependent on grain size and the occurrence of flocculation (Niu et al., 2009). The sinking velocity of barite grains of 1 µm diameter is estimated to range from 8×10^{-5} cm/s for single grains to about 0.02 cm/s for flocs with a total size of 30 µm (Niu et al., 2009), corresponding to about 0.07 to 17 m/d. This is in agreement with the average sinking velocity of sediment trap particles of variable composition, with sizes ranging between 80 and 400 µm, of about 9 m/d (Bach et al., 2012). Given an average ocean depth of 3700 m, pelagic barite grains would thus take between about 0.6 and 150 years to reach the seafloor, during which the barite can potentially equilibrate with the ocean water. Once buried in marine sediments, surrounding pore fluids may be isotopically distinct from pelagic barite (Pretet, 2013), potentially further altering its initial isotopic composition (Middleton et al., 2023b).

Obviously, a number of parameters including temperature, surface area, grain size, porosity, background electrolyte concentration and composition affect the rate of isotope exchange, and thus work with natural pelagic barite and seawater is required for better prediction of exchange rates that may be occurring in marine settings. Nevertheless, the isotope exchange rates estimated here and in earlier works suggest that recrystallization is an important process that must be considered when pelagic barite is used as an environmental archive.

5. Conclusions

In this study, exchange of Ba between natural barite and fluid has been studied by isotopic labelling with ^{135}Ba in batch reactors. Under isotopic equilibrium conditions, isotope fractionation between barite and Ba^{2+} (aq) occurs with $\Delta^{137/134}Ba_{Barite\text{-}Ba2+(aq)} = -0.7 \pm 0.08‰$. The experimental findings suggest that after 756 days of reaction at least 98.7% of Ba in the fluid has been exchanged with the solid. The extent of exchange estimated varies strongly depending on model used, yet all three of the models applied here suggest that isotope exchange was deeper than a few surface layers (between 0.7 and 6.6% of the solid). Based on SEM-observed physical changes on grain surfaces, it can be suggested that dissolution/re-precipitation is the mechanism driving isotope exchange. However, the dissolution-precipitation process did not yield significant variations in grain size as often anticipated with Ostwald ripening.

The experimental results have significant implications for the use of Ba isotopes in pelagic barite as a paleoproxy. Based on the isotope exchange rates estimated in this study, it can be estimated that a complete re-equilibration of an ideal barite cube with an edge size of 1 µm, which is a typical size for pelagic barite, can be achieved within of days to hundreds of years at 25 °C. Despite the uncertainty engendered in this estimation, the estimated rates of isotope exchange suggest that re-equilibration is a process that can significantly impact the isotopic composition of pelagic barite and may have important implications for use of its stable isotope composition for environmental reconstruction purposes.

CRediT authorship contribution statement

Kirsten van Zuilen: Conceptualization, Formal analysis, Methodology, Writing – original draft, Writing – review & editing, Data curation, Visualization. **Anna L. Harrison:** Methodology, Writing – original draft. **Jessica A. Stammeier:** Formal analysis, Writing – original draft. **Thomas F. Nagler:** Writing – original draft. **Vasileios Mavromatis:** Conceptualization, Formal analysis, Funding acquisition, Methodology, Visualization, Writing – original draft, Writing – review & editing.

Declaration of competing interest

The authors declare that they have no known competing financial interests or personal relationships that could have appeared to influence the work reported in this paper.

Data availability

All data used in this study are available in the figures and Supplementary material for online publication.

Acknowledgements

The assistance of Judith Jernej with IC analyses is highly acknowledged. The Raimond Castaing MicroCharacterization centre, particularly Arnaud Proietti, are thanked for their facilitation of SEM analyses. We are thankful to J. Middleton and an anonymous reviewer for their constructive comments on this manuscript. This work has been financially supported by the French national program INSU/LEFE.

Appendix A. Supplementary material

Supplementary material related to this article can be found online at https://doi.org/10.1016/j.epsl.2023.118280.

References

Bach, L.T., Riebesell, U., Sett, S., Febiri, S., Rzepka, P., Schulz, K.G., 2012. An approach for particle sinking velocity measurements in the 3–400 lm size range and considerations on the effect of temperature on sinking rates. Mar. Biol. 159, 1853–1864.

Bates, S.L., Hendry, K.R., Pryer, H.V., Kinsley, C.W., Pyle, K.M., Woodward, E.M.S., Horner, T.J., 2017. Barium isotopes reveal role of ocean circulation on barium cycling in the Atlantic. Geochim. Cosmochim. Acta 204, 286–299.

Bernard, S., Daval, D., Ackerer, P., Pont, S., Meibom, A., 2017. Burial-induced oxygen-isotope re-equilibration of fossil foraminifera explains ocean paleotemperature paradoxes. Nat. Commun. 8, 10.

Blount, C.W., 1977. Barite solubilities and thermodynamic quantities up to 300 degrees C and 1400 bars. Am. Mineral. 62, 942–957.
Böttcher, M.E., Neubert, N., von Allmen, K., Samankassou, E., Nägler, T.F., 2018. Barium isotope fractionation during the experimental transformation of aragonite to witherite and of gypsum to barite, and the effect of ion (de)solvation. Isot. Environ. Health Stud. 54, 324–335.
Bridgestock, L., Hsieh, Y.T., Porcelli, D., Homoky, W.B., Bryan, A., Henderson, G.M., 2018. Controls on the barium isotope compositions of marine sediments. Earth Planet. Sci. Lett. 481, 101–110.
Bridgestock, L., Hsieh, Y.-T., Porcelli, D., Henderson, G.M., 2019. Increased export production during recovery from the Paleocene–Eocene thermal maximum constrained by sedimentary Ba isotopes. Earth Planet. Sci. Lett. 510, 53–63.
Carter, S.C., Paytan, A., Griffith, E.M., 2020. Toward an improved understanding of the marine barium cycle and the application of marine barite as a paleoproductivity proxy. Minerals 10, 421.
Chow, T.J., Goldberg, E.D., 1960. On the marine geochemistry of barium. Geochim. Cosmochim. Acta 20, 192–198.
Christy, A.G., Putnis, A., 1993. The kinetics of barite dissolution and precipitation in water and sodium-chloride brines at 44-85 °C. Geochim. Cosmochim. Acta 57, 2161–2168.
Cisneros-Lazaro, D., Adams, A., Guo, J., Bernard, S., Baumgartner, L.P., Daval, D., Baronnet, A., Grauby, O., Vennemann, T., Stolarski, J., Escrig, S., Meibom, A., 2022. Fast and pervasive diagenetic isotope exchange in foraminifera tests is species-dependent. Nat. Commun. 13, 113.
Cole, D.R., Chakraborty, S., 2001. Rates and mechanisms of isotopic exchange. Rev. Mineral. Geochem. 43, 83–223.
Curti, E., Fujiwara, K., Iijima, K., Tits, J., Cuesta, C., Kitamura, A., Glaus, M.A., Muller, W., 2010. Radium uptake during barite recrystallization at 23 +/- 2 °C as a function of solution composition: an experimental Ba-133 and Ra-226 tracer study. Geochim. Cosmochim. Acta 74, 3553–3570.
De Graaf, S., Lüders, V., Banks, D.A., Sośnicka, M., Reijmer, J.J., Kaden, H., Vonhof, H.B., 2020. Fluid evolution and ore deposition in the Harz Mountains revisited: isotope and crush-leach analyses of fluid inclusions. Miner. Depos. 55, 47–62.
Dehairs, F., Chesselet, R., Jedwab, J., 1980. Discrete suspended particles of barite and the barium cycle in the open ocean. Earth Planet. Sci. Lett. 49, 528–550.
Dietzel, M., Purgstaller, B., Kluge, T., Leis, A., Mavromatis, V., 2020. Oxygen and clumped isotope fractionation during the formation of Mg calcite via an amorphous precursor. Geochim. Cosmochim. Acta 276, 258–273.
Finch, A.A., Allison, N., Steaggles, H., Wood, C.V., Mosselmans, J.F.W., 2010. Ba XAFS in Ba-rich standard minerals and the potential for determining Ba structural state in calcium carbonate. Chem. Geol. 270, 179–185.
Frierdich, A.J., Beard, B.L., Reddy, T.R., Scherer, M.M., Johnson, C.M., 2014a. Iron isotope fractionation between aqueous Fe(II) and goethite revisited: new insights based on a multi-direction approach to equilibrium and isotopic exchange rate modification. Geochim. Cosmochim. Acta 139, 383–398.
Frierdich, A.J., Beard, B.L., Scherer, M.M., Johnson, C.M., 2014b. Determination of the Fe(II) (aq)-magnetite equilibrium iron isotope fractionation factor using the three-isotope method and a multi-direction approach to equilibrium. Earth Planet. Sci. Lett. 391, 77–86.
Frierdich, A.J., Beard, B.L., Rosso, K.M., Scherer, M.M., Spicuzza, M.J., Valley, J.W., Johnson, C.M., 2015. Low temperature, non-stoichiometric oxygen-isotope exchange coupled to Fe(II)-goethite interactions. Geochim. Cosmochim. Acta 160, 38–54.
Géhin, A., Gilbert, B., Chakraborty, S., Stack, A.G., Allard, L.F., Robinet, J.C., Charlet, L., 2021. Long-term C-13 uptake by C-12-enriched calcite. ACS Earth Space Chem. 5, 998–1005.
Gorski, C.A., Fantle, M.S., 2017. Stable mineral recrystallization in low temperature aqueous systems: a critical review. Geochim. Cosmochim. Acta 198, 439–465.
Handler, R.M., Frierdich, A.J., Johnson, C.M., Rosso, K.M., Beard, B.L., Wang, C.M., Latta, D.E., Neumann, A., Pasakarnis, T., Premaratne, W., Scherer, M.M., 2014. Fe(II)-catalyzed recrystallization of goethite revisited. Environ. Sci. Technol. 48, 11302–11311.
Harrison, A.L., Benezeth, P., Schott, J., Oelkers, E.H., Mavromatis, V., 2021. Magnesium and carbon isotope fractionation during hydrated Mg-carbonate mineral phase transformations. Geochim. Cosmochim. Acta 293, 507–524.
Harrison, A.L., Schott, J., Oelkers, E.H., Maher, K., Mavromatis, V., 2022. Rates of carbon and oxygen isotope exchange between calcite and fluid at chemical equilibrium. Geochim. Cosmochim. Acta 335, 369–382.
Harrison, A.L., Heuser, A., Liebetrau, V., Eisenhauer, A., Schott, J., Mavromatis, V., 2023. Equilibrium Ca isotope fractionation and the rates of isotope exchange in the calcite-fluid and aragonite-fluid systems at 25 °C. Earth Planet. Sci. Lett. 603, 117985.
Heberling, F., Metz, V., Bottle, M., Curti, E., Geckeis, H., 2018. Barite recrystallization in the presence of Ra-226 and Ba-133. Geochim. Cosmochim. Acta 232, 124–139.
Hofmann, A.E., Bourg, I.C., Depaolo, D.J., 2012. Ion desolvation as a mechanism for kinetic isotope fractionation in aqueous systems. Proc. Natl. Acad. Sci. USA 109, 18689–18694.
Horner, T.J., Crockford, P.W., 2021. Barium isotopes: drivers, dependencies, and distributions through space and time. In: Elements in Geochemical Tracers in Earth System Science. Cambridge University Press.
Horner, T.J., Kinsley, C.W., Nielsen, S.G., 2015. Barium-isotopic fractionation in seawater mediated by barite cycling and oceanic circulation. Earth Planet. Sci. Lett. 430, 511–522.
Horner, T.J., Pryer, H.V., Nielsen, S.G., Crockford, P.W., Gauglitz, J.M., Wing, B.A., Ricketts, R.D., 2017. Pelagic barite precipitation at micromolar ambient sulfate. Nat. Commun. 8, 11.
Hsieh, Y.T., Henderson, G.M., 2017. Barium stable isotopes in the global ocean: tracer of Ba inputs and utilization. Earth Planet. Sci. Lett. 473, 269–278.
Johnson, C.M., Skulan, J.L., Beard, B.L., Sun, H., Nealson, K.H., Braterman, P.S., 2002. Isotopic fractionation between Fe(III) and Fe(II) in aqueous solutions. Earth Planet. Sci. Lett. 195, 141–153.
Kang, J.T., Bracco, J.N., Rimstidt, J.D., Zhu, G.H., Huang, F., Zhu, C., 2022. Ba attachment and detachment fluxes to and from barite surfaces in ^{137}Ba-enriched solutions with variable $[Ba^{2+}]/[SO_4^{2-}]$ ratios near solubility equilibrium. Geochim. Cosmochim. Acta 317, 180–200.
Liu, Z., Rimstidt, J.D., Zhang, Y., Yuan, H., Zhu, C., 2016. A stable isotope doping method to test the range of applicability of detailed balance. Geochem. Perspect. Lett. 2, 78–86.
Maher, K., Johnson, N.C., Jackson, A., Lammers, L.N., Torchinsky, A.B., Weaver, K.L., Bird, D.K., Brown, G.E., 2016. A spatially resolved surface kinetic model for forsterite dissolution. Geochim. Cosmochim. Acta 174, 313–334.
Martinez-Ruiz, F., Paytan, A., Gonzalez-Munoz, M.T., Jroundi, F., Abad, M.M., Lam, P.J., Horner, T.J., Kastner, M., 2020. Barite precipitation on suspended organic matter in the mesopelagic zone. Front. Earth Sci. 8, 17.
Mavromatis, V., Gautier, Q., Bosc, O., Schott, J., 2013. Kinetics of Mg partition and Mg stable isotope fractionation during its incorporation in calcite. Geochim. Cosmochim. Acta 114, 188–203.
Mavromatis, V., van Zuilen, K., Purgstaller, B., Baldermann, A., Nägler, T.F., Dietzel, M., 2016. Barium isotope fractionation during witherite ($BaCO_3$) dissolution, precipitation and at equilibrium. Geochim. Cosmochim. Acta 190, 72–84.
Mavromatis, V., Harrison, A.L., Eisenhauer, A., Dietzel, M., 2017. Strontium isotope fractionation during strontianite ($SrCO_3$) dissolution, precipitation and at equilibrium. Geochim. Cosmochim. Acta 218, 201–214.
Mavromatis, V., van Zuilen, K., Blanchard, M., van Zuilen, M., Dietzel, M., Schott, J., 2020. Experimental and theoretical modelling of kinetic and equilibrium Ba isotope fractionation during calcite and aragonite precipitation. Geochim. Cosmochim. Acta 269, 566–580.
Mavromatis, V., Purgstaller, B., Louvat, P., Faure, L., Montouillout, V., Gaillardet, J., Schott, J., 2021. Boron isotope fractionation during the formation of amorphous calcium carbonates and their transformation to Mg-calcite and aragonite. Geochim. Cosmochim. Acta 315, 152–171.
McManus, J., Berelson, W.M., Klinkhammer, G.P., Johnson, K.S., Coale, K.H., Anderson, R.F., Kumar, N., Burdige, D.J., Hammond, D.E., Brumsack, H.J., McCorkle, D.C., Rushdi, A., 1998. Geochemistry of barium in marine sediments: implications for its use as a paleoproxy. Geochim. Cosmochim. Acta 62, 3453–3473.
Middleton, J.T., Hong, W.-L., Paytan, A., Auro, M.E., Griffith, E.M., Horner, T.J., 2023a. Barium isotope fractionation in barite–fluid systems at chemical equilibrium. Chem. Geol. 627, 121453.
Middleton, J.T., Paytan, A., Auro, M.E., Saito, M.A., Horner, T.J., 2023b. Barium isotope signatures of barite–fluid ion exchange in Equatorial Pacific sediments. Earth Planet. Sci. Lett. 612, 118150.
Monnin, C., Cividini, D., 2006. The saturation state of the world's ocean with respect to (Ba, Sr)SO4 solid solutions. Geochim. Cosmochim. Acta 70, 3290–3298.
Niu, H., Drozdowski, A., Husain, T., Veitch, B., Bose, N., Lee, K., 2009. Modeling the dispersion of drilling muds using the bblt model: the effects of settling velocity. Environ. Model. Assess. 14, 585–594.
Oelkers, E.H., Benning, L.G., Lutz, S., Mavromatis, V., Pearce, C.R., Plümper, O., 2015. The efficient long-term inhibition of forsterite dissolution by common soil bacteria and fungi at Earth surface conditions. Geochim. Cosmochim. Acta 168, 222–235.
Oelkers, E.H., Berninger, U.N., Perez-Fernandez, A., Chmeleff, J., Mavromatis, V., 2018. The temporal evolution of magnesium isotope fractionation during hydromagnesite dissolution, precipitation, and at equilibrium. Geochim. Cosmochim. Acta 226, 36–49.
Oelkers, E.H., von Strandmann, P., Mavromatis, V., 2019. The rapid resetting of the Ca isotopic signatures of calcite at ambient temperature during its congruent dissolution, precipitation, and at equilibrium. Chem. Geol. 512, 1–10.
Paytan, A., Griffith, E.M., 2007. Marine barite: recorder of variations in ocean export productivity. Deep-Sea Res., Part 2, Top. Stud. Oceanogr. 54, 687–705.
Paytan, A., Kastner, M., 1996. Benthic Ba fluxes in the central Equatorial Pacific, implications for the oceanic Ba cycle. Earth Planet. Sci. Lett. 142, 439–450.
Pearce, C.R., Saldi, G.D., Schott, J., Oelkers, E.H., 2012. Isotopic fractionation during congruent dissolution, precipitation and at equilibrium: evidence from Mg isotopes. Geochim. Cosmochim. Acta 92, 170–183.
Perez-Fernandez, A., Berninger, U.N., Mavromatis, V., Pogge von Strandmann, P.A.E., Oelkers, E.H., 2017. Ca and Mg isotope fractionation during the stoichiometric dissolution of dolomite at temperatures from 51 to 126 °C and 5bars CO_2 pressure. Chem. Geol. 467, 76–88.
Persson, I., Sandstrom, M., Yokoyama, H., Chaudhry, M., 1995. Structure of the solvated strontium and barium ions in aqueous, dimethyl-sulfoxide and pyridine

solution, and crystal-structure of strontium and barium hydroxide octahydrate. Z. Naturforsch. A, J. Phys. Sci. 50, 21–37.
Pretet, C., 2013. Non-Traditional Isotopes (Barium and Calcium) and Elemental Ratios in Scleractinian Coral Skeleton: New Look into Geochemical Cycles, Environmental Proxies and Bio-Calcification Processes. Doctoral Thesis. Université de Genève, p. 4584.
Schauble, E.A., 2004. Applying stable isotope fractionation theory to new systems. Rev. Mineral. Geochem. 55, 65–111.
Schott, J., Pokrovsky, O.S., Oelkers, E.H., 2009. The link between mineral dissolution/precipitation kinetics and solution chemistry. Rev. Mineral. Geochem. 70, 207–258.
Schott, J., Mavromatis, V., Fujii, T., Pearce, C.R., Oelkers, E.H., 2016. The control of carbonate mineral Mg isotope composition by aqueous speciation: theoretical and experimental modeling. Chem. Geol. 445, 120–134.
Skulan, J.L., Beard, B.L., Johnson, C.M., 2002. Kinetic and equilibrium Fe isotope fractionation between aqueous Fe(III) and hematite. Geochim. Cosmochim. Acta 66, 2995–3015.
Stamm, F.M., Zambardi, T., Chmeleff, J., Schott, J., von Blanckenburg, F., Oelkers, E.H., 2019. The experimental determination of equilibrium Si isotope fractionation factors among $H_4SiO_4^0$, $H_3SiO_4^-$ and amorphous silica ($SiO_2 \cdot 0.32\ H_2O$) at 25 and 75 °C using the three-isotope method. Geochim. Cosmochim. Acta 255, 49–68.
Tang, J., Dietzel, M., Boehm, F., Koehler, S.J., Eisenhauer, A., 2008. Sr^{2+}/Ca^{2+} and $^{44}Ca/^{40}Ca$ fractionation during inorganic calcite formation: II. Ca isotopes. Geochim. Cosmochim. Acta 72, 3733–3745.
Torres, M.E., Brumsack, H.J., Bohrmann, G., Emeis, K.C., 1996. Barite fronts in continental margin sediments: a new look at barium remobilization in the zone of sulfate reduction and formation of heavy barites in diagenetic fronts. Chem. Geol. 127, 125–139.
van Zuilen, K., Muller, T., Nagler, T.F., Dietzel, M., Kusters, T., 2016a. Experimental determination of barium isotope fractionation during diffusion and adsorption processes at low temperatures. Geochim. Cosmochim. Acta 186, 226–241.
van Zuilen, K., Nagler, T.F., Bullen, T.D., 2016b. Barium isotopic compositions of geological reference materials. Geostand. Geoanal. Res. 40, 543–558.
von Allmen, K., Bottcher, M.E., Samankassou, E., Nagler, T.F., 2010. Barium isotope fractionation in the global barium cycle: first evidence from barium minerals and precipitation experiments. Chem. Geol. 277, 70–77.
Wang, W., Wu, Z., Huang, F., 2021. Equilibrium barium isotope fractionation between minerals and aqueous solution from first-principles calculations. Geochim. Cosmochim. Acta 292, 64–77.
Wiederhold, J.G., Kraemer, S.M., Teutsch, N., Borer, P.M., Halliday, A.N., Kretzschmar, R., 2006. Iron isotope fractionation during proton-promoted, ligand-controlled, and reductive dissolution of goethite. Environ. Sci. Technol. 40, 3787–3793.
Zhang, Q., Peng, X., Nie, Y., Zheng, Q., Shangguan, J., Zhu, C., Bustillo, K.C., Ercius, P., Wang, L., Limmer, D.T., Zheng, H., 2022. Defect-mediated ripening of core-shell nanostructures. Nat. Commun. 13, 2211.
Zhen-Wu, B.Y., Dideriksen, K., Olsson, J., Raahauge, P.J., Stipp, S.L.S., Oelkers, E.H., 2016. Experimental determination of barite dissolution and precipitation rates as a function of temperature and aqueous fluid composition. Geochim. Cosmochim. Acta 194, 193–210.
Zheng, X.Y., Beard, B.L., Reddy, T.R., Roden, E.E., Johnson, C.M., 2016. Abiologic silicon isotope fractionation between aqueous Si and Fe(III)-Si gel in simulated Archean seawater: implications for Si isotope records in Precambrian sedimentary rocks. Geochim. Cosmochim. Acta 187, 102–122.